A. Ozgurluk and C. T.-C. Nguyen, "On-Chip Precision Residual Strain Diagnostic Based on Gap-Dependent Electrical Stiffness", *Proc. Int. Conf. Solid-State Sens., Actuators, Microsyst. Tech. Dig. (Transducers)*, Berlin, Germany, Jun. 2019, pp.2029-2032.

ON-CHIP PRECISION RESIDUAL STRAIN DIAGNOSTIC BASED ON GAP-DEPENDENT ELECTRICAL STIFFNESS

Alper Ozgurluk, and Clark T.-C. Nguyen
Department of EECS, University of California at Berkeley, Berkeley, CA, USA

ABSTRACT

An on-chip strain measurement device is demonstrated that harnesses precision frequency measurement to precisely extract sub-nm displacements, allowing it to determine the residual strain in a given structural film with best-in-class accuracy, where stress as small as 15MPa corresponds to 2.9nm of displacement. The approach specifically harnesses a spoke-supported ring structure (*cf.* Fig. 1) surrounded both inside and outside by balanced capacitive-gap transducers that pull its resonance frequency according to strain-induced changes in inner and outer electrode-to-structure gap spacing. The use of a ring structure with balanced electrodes further eliminates uncertainty in the starting gap spacing, which in turn enhances accuracy. The importance of attaining such accuracy manifests in the fact that knowledge of residual strain might be the single most important constraint on the complexity of large mechanical circuits, such as the mechanical filter of [1].

KEYWORDS

Strain sensor, electrical stiffness, on-chip, polysilicon, mechanical resonator, ring, mechanical circuit.

INTRODUCTION

Recent demonstrations of sub-20nm electrode-to-resonator gaps have permitted capacitive-gap transducer electromechanical coupling strengths well past those posted by alternatives in the high (HF) to very high frequency (VHF) range, with C_x/C_o's up to 71% at 10-MHz [2] and 1.62% at 60-MHz [3]. These compare quite favorably with the 0.86% of alternatives [4], all while preserving comparatively larger Q's, e.g., 30000 versus 2100. Unfortunately, such performance comes with a price—in this case, greater susceptibility to stress. Indeed, thermal expansion-derived strain impacts small gaps much more than large ones, to point of debilitating large mechanical circuits of small-gapped resonators in the absence of defensive measures.

Interestingly, accurate knowledge of strain might be the single most important constraint on the ultimate size and performance of an array-based mechanical circuit like that of [5]. For example, finite element analysis (FEA) on a 6-disk coupled linear array under different compressive stress levels (*cf.* Fig. 2) shows that end resonators displace the most, i.e., 20nm at 200MPa, while the inner ones barely move, i.e., 6nm at 200MPa. The mechanical channel-select filter of [5] takes advantage of this by removing the electrodes around the end resonators (that would otherwise short) and using them as buffers to suppress the strain-derived displacement for the inner disks. Although this buffering method is effective for the array of 40-nm-gap devices in [5], it will not suffice for ultra-small gaps, i.e., sub-5nm, which are on the horizon. The desire for gaps like this

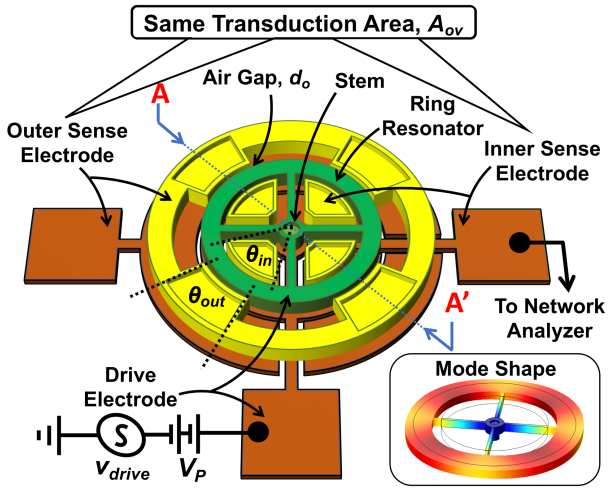

Fig. 1: The ring-based strain sensor described herein in a typical operating circuit with dimensions given in Table I. The inset shows the finite element analysis (FEA) simulated mode shape.

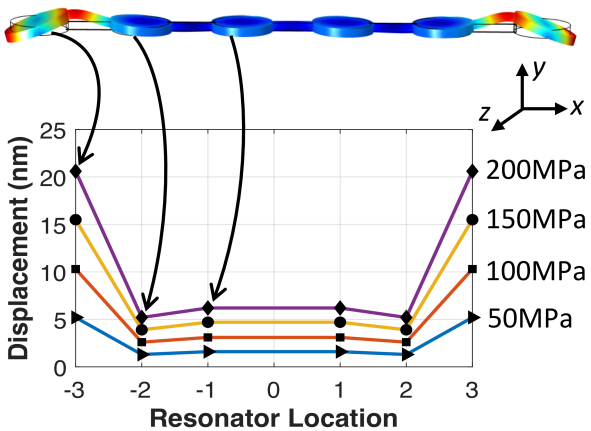

Fig. 2: Finite-element simulated plot of strain-induced x-axial displacement versus location for disks in a 6-disk polysilicon mechanically-coupled array under various compressive residual stress levels.

amplify the need to minimize post-fabrication residual strain—a need that will likely spur extensive fabrication recipe optimization, which in turn calls for a very sensitive, high resolution strain diagnostic tool.

Unfortunately, existing residual strain measurement techniques—including wafer bow [6] and various on-chip approaches [7], [8], [9]—either lack the precision to permit the most aggressive mechanical circuit designs or require large footprint area. For example, the Vernier stress gauge of [9] uses visual readout of indicator beam movement under a microscope, which is inherently imprecise. In addition, its sensitivity is directly proportional to its indicator beam length, which acts as a lever to amplify Vernier

A. Ozgurluk and C. T.-C. Nguyen, "On-Chip Precision Residual Strain Diagnostic Based on Gap-Dependent Electrical Stiffness", *Proc. Int. Conf. Solid-State Sens., Actuators, Microsyst. Tech. Dig. (Transducers)*, Berlin, Germany, Jun. 2019, pp.2029-2032.

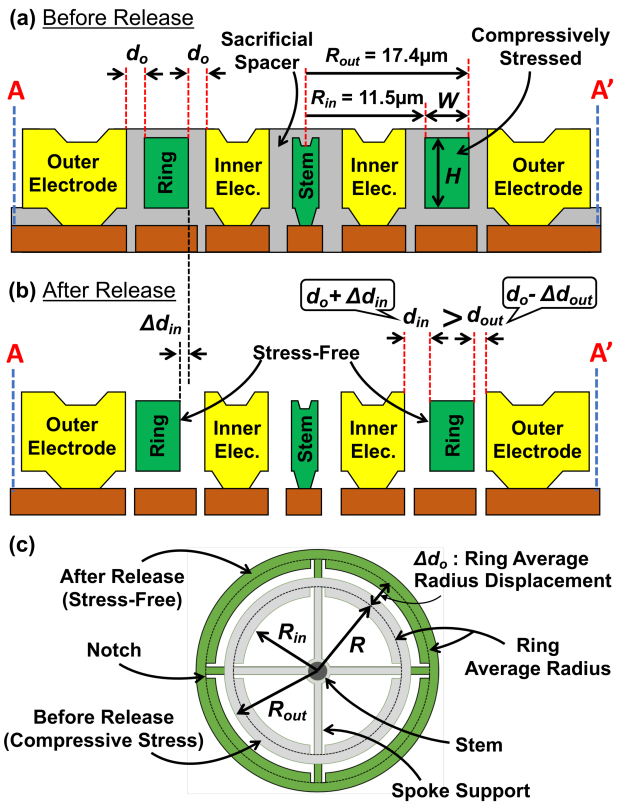

Fig. 3: Cross-sections through AA' in Fig. 1 (a) before release (b) after release. (c) Top view before and after release.

movement. Apart from occupying a large die area, the 100μm-long beam lengths need to measure stress down to 15MPa are susceptible to stiction and vertical stress gradients that bend them out of plane, rendering them unusable.

Pursuant to providing a more capable strain sensor, this paper presents an on-chip, spoke-supported ring-based strain measurement structure, shown in Fig. 1, that harnesses precision frequency measurement to precisely extract sub-nm displacements, allowing it to determine the residual strain in a given structural film with unprecedented accuracy, with measured stresses as small as 15MPa.

DEVICE STRUCTURE AND OPERATION

The strain sensor comprises a spoke-supported doped polysilicon ring surrounded by matched inner and outer doped polysilicon electrodes [10]. The device conveniently fabricates alongside tiny-gap mechanical filters via the process of [5], making it well-suited for diagnostic (or real-time) gap-control applications. Fig. 3(a) presents the cross-section of the strain sensor at the process step immediately before release, where a sacrificial oxide encases its ring structure on all sides. At this point, the electrode edges would ideally be the sidewall sacrificial oxide thickness d_o from the ring edges. In this state, the film is under stress due to thermal expansion differences with the substrate that manifest upon cooling from the deposition temperature to room temperature.

Removal of sacrificial oxide (via hydrofluoric acid) releases not only the structure, but also the stress, allowing the structure and substrate-anchored electrodes to freely

Table 1: Geometric dimensions and material properties

Parameter	Value	Parameter	Value
Inner Radius, R_{in}	17.4μm	Outer Radius, R_{out}	11.5μm
Inner Angle, θ_{in}	65.26°	Outer Angle, θ_{out}	43.13°
Inner Coeff., χ_{in}	0.912	Outer Coeff., χ_{out}	1.075
Thickness, H	3μm	Young's Modulus	158GPa
Ring Width, W	5.9μm	Density	2300kg/m³
Ring Radius, R	14.45μm	Poisson Ratio	0.226

displace relative to one another (*cf.* Fig. 3(b)) according to the value of residual strain ε, which takes the form

$$\varepsilon = \frac{\sigma}{E} = \frac{\Delta d_o}{R} \tag{1}$$

where σ is the residual stress, E is the Young's modulus of the resonator material, R is the distance from the stem to the center of the ring width, i.e., average ring radius in Fig. 3(c), and Δd_o is the strain-induced radial displacement at the average ring radius, given by

$$\Delta d_o = d_{out} - d_o = d_o - d_{in} \tag{2}$$

Equation (1) indicates a linear relationship between strain and actuation gap for small displacements, where measuring strain essentially amounts to measuring Δd_o. The small size of the proposed structure (*cf.* Table 1) predicates gap changes on the order of 1nm, which require a very sensitive measurement method. Here, frequency-based metrology employing the bias, excitation, and sensing scheme shown in Fig. 1 offers an excellent approach.

Specifically, when the electrode-to-resonator gaps are small, the resonance frequency of the ring structure becomes a strong function of electrical stiffness, which is in turn strongly dependent on gap spacing. Here, the expression for resonance frequency takes the form

$$f_{in(out)} = \sqrt{f_{nom}^2 - \frac{\varepsilon_o V_p^2}{2\pi^3 \rho W R} \frac{R_{in(out)}\theta_{in(out)}}{\chi_{in(out)} d_{in(out)}^3}} \tag{3}$$

where ε_o is the free-space permittivity, ρ is the density of the structural material, V_p is the dc-bias voltage, $R_{in(out)}$ is the distance from inner (outer) edge of the annulus to the stem, $d_{in(out)}$ is the inner (outer) electrode actuation gap, $\theta_{in(out)}$ is the inner (outer) electrode subtended angle in radians, W is the annulus width, $\chi_{in(out)}$ is a mass modifier factor relating the actual physical mass to the dynamic mass at the inner (outer) edge of the annulus, and f_{nom} is the mechanical (or nominal) resonance frequency for the ring, i.e. with no applied voltages [10].

Given this, measuring gap change (hence, strain) entails first measuring the resonance frequency of the ring for various dc-bias voltages V_P applied between the ring and either the inner or outer electrode, then curve fitting via (3) to obtain f_{nom} and either d_{in} or d_{out}. Δd_o is then the difference between this extracted gap and the nominal gap, d_o. Although quite straightforward, one issue limiting the accuracy with

A. Ozgurluk and C. T.-C. Nguyen, "On-Chip Precision Residual Strain Diagnostic Based on Gap-Dependent Electrical Stiffness", *Proc. Int. Conf. Solid-State Sens., Actuators, Microsyst. Tech. Dig. (Transducers)*, Berlin, Germany, Jun. 2019, pp.2029-2032.

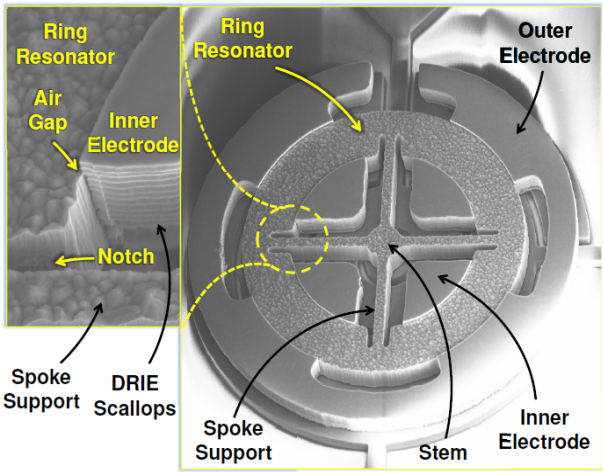

Fig. 4: SEM of a fabricated polysilicon strain diagnostic device.

this approach is its dependence on the initial gap, d_o determined by the sidewall sacrificial layer deposition thickness, which could deviate from the target. To quantify this, a 1nm uncertainty in the initial gap, hence Δd_o, causes 69.2με error in strain, or 10.9MPa in stress for polysilicon, using (1) with the parameters given in Table 1. Considering that target stresses might be as small as 15MPa, this much error is not acceptable and calls for a better stress extraction technique independent of the starting gap, d_o.

Recognizing that after release the outer electrode gap shrinks (expands) as much as the inner electrode expands (shrinks), a balanced measurement entailing separate extraction of inner and outer electrode gaps, d_{in} and d_{out}, respectively, removes the dependency on the initial gap according to

$$\Delta d_o = \frac{d_{out} - d_{in}}{2} \tag{4}$$

Substituting (4) into (1) yields the residual strain, ε

$$\varepsilon = \frac{\sigma}{E} = \frac{d_{out} - d_{in}}{2R} \tag{5}$$

As will be seen, the dependence is strong enough and frequency measurement precision good enough that even sub-nm gap changes are precisely measurable.

EXPERIMENTAL RESULTS

Fig. 4 presents wide- and zoomed-view SEM's of a ring-based residual strain gauge (which was fabricated alongside tiny-gap mechanical filters). Fig. 5 presents vacuum-measured transmission spectra for the ring operating in its first mode shape (*cf.* inset of Fig. 1) while driven (a) via inner electrodes only and (b) via outer electrodes only. The difference in frequency excursion for each case indicates a difference in electrode-to-resonator gap spacing that extracts very precisely upon curve-fitting the data, as done in Fig. 6. Here, the inner gap is 43.1nm, while the outer 40.2nm. These comprise directional changes from the extracted starting 41.65-nm gap that very precisely indicate 15.05MPa of compressive residual stress. Opposite gap changes, i.e., the inner gap decreasing and outer gap

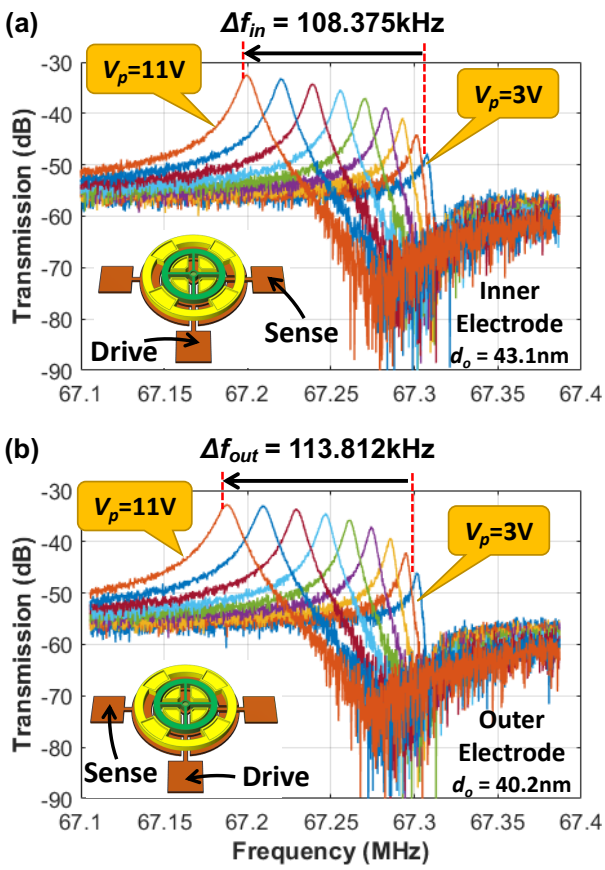

Fig. 5: Measured frequency spectra for a ring strain diagnostic device as a function of dc-bias voltage using the (a) inner and (b) outer port for sensing.

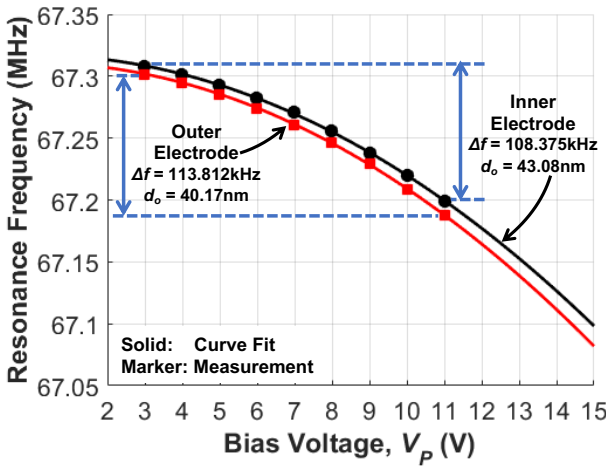

Fig. 6: Measured frequency versus dc-bias voltage curves with curve-fits to extract electrode-to-resonator gaps.

increasing, would indicate tensile stress, and would be measurable just as precisely.

Scale Factor (Sensitivity)

Scale factor (or sensitivity) for a resonant sensor is a measure of its frequency shift per unit strain, here simply corresponding to the slope of the resonance frequency vs. strain curve before any gap change takes place, i.e., when $d_{in} = d_{out} = d_o$, as follows

A. Ozgurluk and C. T.-C. Nguyen, "On-Chip Precision Residual Strain Diagnostic Based on Gap-Dependent Electrical Stiffness", *Proc. Int. Conf. Solid-State Sens., Actuators, Microsyst. Tech. Dig. (Transducers)*, Berlin, Germany, Jun. 2019, pp.2029-2032.

$$\left(\frac{\partial f_o}{\partial \varepsilon}\right)_{in(out)} = -(+)\frac{3\varepsilon_o V_P^2}{4\pi^3 \rho W f_{nom}} \frac{R_{in(out)}\theta_{in(out)}}{\chi_{in(out)} d_o^4} \quad (6)$$

Note that in (6) positive strain corresponds to tensile stress, while negative to compression. The aforementioned balanced measurement scheme further enhances the scale factor according to

$$\frac{\partial f_o}{\partial \varepsilon} = \left(\frac{\partial f_o}{\partial \varepsilon}\right)_{out} - \left(\frac{\partial f_o}{\partial \varepsilon}\right)_{in} \quad (7)$$

Noting that the overlap area, A_{ov} for the inner and outer electrodes are the same using the values in Table 1 and substituting (6) in (7) yields

$$\frac{\partial f_o}{\partial \varepsilon} = \frac{3\varepsilon_o V_P^2 A_{ov}}{2\pi^3 \rho W H f_{nom} d_o^4} \quad (8)$$

The fourth power inverse dependence of the scale factor on the actuation gap d_o makes this sensor extremely sensitive considering its ~40nm gaps. Eq. (8) in fact predicts a scale factor of 291.54 Hz/με for the strain sensor of Fig. 1 with the parameters outlined in Table 1 under 11V dc-bias.

Resolution

Resolution is the minimum strain that the sensor of Fig. 1 can accurately measure through its transduction mechanism, i.e., strain to frequency conversion. Here, the minimum resolvable resonance frequency shift—largely governed by the resonator's short-term frequency stability—sets the lower resolution limit. Fortunately, the high Q of capacitive-gap polysilicon resonators at HF permit them to exhibit excellent short-term stability [12], [13]. In particular, the 61-MHz wine-glass disk resonator of [13] posts an Allan deviation, σ_{ymin} of 2×10^{-8} at 1s integration time. Given Allan deviation, the expression for frequency jitter Δf takes the form

$$\Delta f = \sigma_{ymin} f_o \quad (9)$$

The resolution, $\Delta\varepsilon$ is then

$$\Delta\varepsilon = \Delta f \left(\frac{\partial f_o}{\partial \varepsilon}\right)^{-1}_{in(out)} \quad (10)$$

Finally, substituting (6) and (9) in (10) yields

$$\Delta\varepsilon = \sigma_{ymin} f_o \frac{4\pi^3 \rho W H f_{nom}}{3\varepsilon_o V_P^2 A_{ov}} d_o^4 \quad (11)$$

If one supposes the ring resonator herein posts the Allan deviation performance of the wine-glass disk in [13], then (11) with the parameters in Table 1 and assuming an 11V dc-bias yields for resolution 9.19nε. Of course, this is a calculated value that requires measured verification. But if real, it bests many other published on-chip strain sensors, as shown in Table 2.

Range

The initial gap, d_o determines maximum permissible strain-induced ring displacement. The corresponding maximum measurable strain ε_{max} then follows by taking $\Delta d_o = d_o$ in (1), which yields

$$\varepsilon_{max} = \frac{d_o}{R} \quad (12)$$

Table 2: Performance comparison chart with state-of-the-art strain sensors

Technology	MEMS Cap. [14]	MEMS Piezo. [15]	MEMS Res. [16]	This Work	Unit
Scale Factor	816μV	340μV	120Hz	292Hz	$\mu\varepsilon^{-1}$
Resolution	870	28.7	4	9.19	nε
Range	±1000	N/A	±2.5	±2768	με

Using (12), the device of this work with an initial gap of 40nm has a maximum measurable strain of ±2768με, which corresponds to ±415.2MPa of stress for polysilicon.

CONCLUSIONS

The frequency output provided by gap-dependent electrical stiffness permits the strain sensor described herein to achieve a combination of small size, large scale factor, low resolution, and large measurement range, that outpace alternatives, in some cases by substantial margins. Although the described sensor tailors specifically to tiny-gap devices, it is not difficult to see that its underlying approach will work regardless of the process or gap used.

Although presented as a diagnostic tool, this device is clearly applicable as a general strain sensor. Indeed, its small size and high performance make it a strong candidate for use as an *in situ* strain sensor that might measure real-time strain changes—due to package stress, thermal variations, or other sources—to then allow real-time corrections. Such an approach could play a significant role towards improving the long-term stability of capacitive-gap transduced oscillators beyond their already impressive marks [13], [17].

REFERENCES:

[1] A. Ozgurluk et al., "RF channel-select micromechanical disk filters ...," DOI: 10.1109/TUFFC.2018.2881727.
[2] A. Ozgurluk et al., "Widely tunable 20-nm-gap ruthenium metal square-plate resonator," MEMS 2019.
[3] J. N. Nilchi et al., "High Cx/Co 13nm-capacitive-gap transduce ...," DOI: 10.1109/MEMSYS.2017.7863560.
[4] G. Piazza et al., "Piezoelectric aluminum nitride vibrating contour ...," DOI: 10.1109/JMEMS.2006.889503.
[5] M. Akgul et al., " RF channel-select micromechanical disk filters, pa …," DOI: 10.1109/TUFFC.2018.2883296.
[6] J. Lu, Handbo…, Lulburn, GA: Fairmount Press, 1996
[7] H. Guckel et al., "Diag ...," DOI: 10.1088/0960-1317/2/2/004.
[8] W. Fang et al., "P…," DOI: 10.1088/0960-1317/4/3/004.
[9] L. Lin et al., "A micro …," DOI: 10.1109/84.650128.
[10] T. L. Naing et al., "High-Q UHF spoke-supported ring resonators," DOI: 10.1109/JMEMS.2015.2480395.
[11] W.-T. Hsu et al., "Stiffness-compensated temperature-insensi ...," DOI: 10.1109/MEMSYS.2002.984374.
[12] Y.-W. Lin et al., "Series-resonant VHF micromechanica …," DOI: 10.1109/JSSC.2004.837086
[13] T. O. Rocheleau et al., "Long-term stability of a hermeticall…," DOI: 10.1109/EFTF-IFC.2013.6702095
[14] M. Suster et al., "A…," DOI: 10.1109/ISSCC.2007.373453.
[15] S. Kon et al., "A hi…," DOI: 10.1109/JSEN.2008.2006708.
[16] L. Belsito et al., "High rsolution strain sensing on steel by s …," DOI: 10.1109/Transducers.2013.6626936.
[17] SiTime SiT5358 DataSheet.